*J. Anat.* (1999) **195**, pp. 341–357, with 8 figures Printed in the United Kingdom


# Localisation and quantitation of autonomic innervation in the porcine heart I: conduction system

**SIMON J. CRICK[1], MARY N. SHEPPARD[2], SIEW YEN HO[1] AND ROBERT H. ANDERSON[1]**

[1] *Section of Paediatrics, National Heart & Lung Institute, Royal Brompton Campus, Imperial College of Science, Technology & Medicine, and* [2] *Department of Pathology, Royal Brompton Hospital, London, UK*

(*Accepted 18 May 1999*)

ABSTRACT

This study was prompted by the prospect of transgenic pigs providing donor hearts for transplantation in human recipients. Autonomic innervation is important for the control of cardiac dynamics, especially in the conduction system. Our objective was to assess the relative distribution of autonomic nerves in the pig heart, focusing initially on the conduction system but addressing also the myocardium, endocardium and epicardium (see Crick et al. 1999). Quantitative immunohistochemical and histochemical techniques were adopted. All regions of the conduction system possessed a significantly higher relative density of the total neural population immunoreactive for the general neuronal marker protein gene product 9.5 (PGP 9.5) than did the adjacent myocardium. A similar density of PGP 9.5-immunoreactive innervation was observed between the sinus node, the transitional region of the atrioventricular node, and the penetrating atrioventricular bundle. A differential pattern of PGP 9.5-immunoreactive innervation was present within the atrioventricular node and between the components of the ventricular conduction tissues, the latter being formed by an intricate network of Purkinje fibres. Numerous ganglion cell bodies were present in the peripheral regions of the sinus node, in the tissues of the atrioventricular groove, and even in the interstices of the compact atrioventricular node. Acetylcholinesterase (AChE)-containing nerves were the dominant subpopulation observed, representing 60–70% of the total pattern of innervation in the nodal tissues and penetrating atrioventricular bundle. Tyrosine hydroxylase (TH)-immunoreactive nerves were the next most abundant neural subpopulation, representing 37% of the total pattern of innervation in the compact atrioventricular node compared with 25% in the transitional nodal region. A minor population of ganglion cell bodies within the atrioventricular nodal region displayed TH immunoreactivity. The dominant peptidergic nerve supply possessed immunoreactivity for neuropeptide Y (NPY), which displayed a similar pattern of distribution to that of TH-immunoreactive nerve fibres. Calcitonin gene-related peptide (CGRP)-immunoreactive nerves represented 8–9% of the total innervation of the nodal tissues and penetrating atrioventricular bundle, increasing to 14–19% in the bundle branches. Somatostatin-immunoreactive nerve fibres were relatively sparse (4–13% of total innervation) and were most abundant in the nodes, especially the compact atrioventricular node. The total pattern of innervation of the porcine conduction system was relatively homogeneous. A substantial proportion of nerve fibres innervating the nodal tissues could be traced to intracardiac ganglia indicative of an extensive intrinsic supply. The innervation of the atrioventricular node and ventricular conduction tissues was similar to that observed in the bovine heart, but markedly different to that of the human heart. It is important that we are aware of these findings in view of the future use of transgenic pig hearts in human xenotransplantation.

*Key words*: Cardiac conduction system; autonomic nervous system; xenotransplantation.

Correspondence to Dr Simon J. Crick, Section of Paediatrics (Cardiac Morphology), National Heart & Lung Institute, Imperial College School of Medicine, Dovehouse Street, London, SW3 6LY, United Kingdom. Tel.: +44 (0) 171 352 8121, ext. 2253; fax: (0) 171 351 8230; e-mail: s.crick@ic.ac.uk

## INTRODUCTION

The pig is, perhaps, now one of the most important models for cardiovascular research (Hughes, 1986). In clinical terms, porcine cardiac valves have been utilised for many years in the surgical replacement of diseased human valves. More recently, however, the pig has swept to the forefront of transplantation medicine, with the development and successful breeding of transgenic pigs that possess human genes capable of preventing the rejection of porcine transplanted organs within human recipients (White & Wallwork, 1993; Cozzi & White, 1995). Rapid advances in transgenic technology have potentially solved many of the immunological difficulties of using pig organs to support life in a human being. Nevertheless, other difficulties still remain. Our recent comparative study revealed several significant anatomical and morphological differences between normal human and pig hearts (Crick et al. 1998), contradicting the previous acceptance in the literature that their cardiac anatomies were almost identical (Douglas, 1972; Hughes, 1986; Cooper et al. 1991; White & Wallwork, 1993). These reported differences are, in part, attributable to the fact that pigs are quadrupeds whereas man is bipedal. The contrast in stance creates differing demands on their respective circulatory systems and this has resulted in the anatomical and/or morphological adaptations of their respective hearts. Cardiac dynamics are under stringent control of the autonomic nervous system. Differences in anatomy may, therefore, reflect similar differences in the pattern of cardiac innervation.

Previous studies in the conduction system of man (Crick et al. 1994), cattle (Crick et al. 1996*a*) and guinea pigs (Crick et al. 1996*b*) have revealed interesting variations in the extent of autonomic neural subpopulations. The conduction system of the porcine heart is well developed, as in other ungulate species, and possesses a characteristic dense network of Purkinje fibres forming its ventricular conduction system. Some electrophysiological studies have been carried out on the conduction system of the pig. Opthof et al. (1987) described the functional morphology of the porcine sinus node, whilst other studies evaluated the pacing parameters and the retrograde ventriculoatrial conduction within the atrioventricular conduction axis (Bowman & Hughes, 1984*a*, *b*). Despite the interest in the cardiac electrophysiology of the pig, very little attention has been focused on the innervation of the porcine conduction system. Nevertheless, there have been histochemical investigations of the porcine arterial (De Biasi & Vitellaro-Zuccarello, 1982) and atrioventricular valves (De Biasi et al. 1984), which demonstrated the presence of complex cholinergic and adrenergic plexuses throughout the endocardial surfaces of the valve leaflets. Other studies have described the morphology of nerve endings within the endocardium of both young pigs (Tranum-Jensen, 1975) and of pig fetuses (Macdonald et al. 1983), together with their afferent connections within the brainstem (Hopkins et al. 1984). Furthermore, the electrophysiological properties of cultured intrinsic cardiac neurons from neonatal pigs have suggested that the cardiac ganglionated plexus represents a distinct population of autonomic neurons which may be capable of intracardiac integration of efferent information to the heart, and even independent activity (Smith et al. 1992). This suggests that the porcine heart is supplied by an extensive system of intrinsic nerves, as well as those of efferent origin, in this way differing markedly from the human heart, which possesses relatively few intracardiac ganglia (Singh et al. 1996; Armour et al. 1997).

This study, therefore, describes the morphology and quantitative distribution of innervation of the porcine conduction system, whereas the accompanying paper (Crick et al. 1999) evaluates the overall distribution of autonomic nerves within the endocardium, myocardium and epicardium of the pig heart.

## MATERIALS AND METHODS

### *Tissue collection and processing*

Fresh young adult pig hearts (n = 8; aged 3–6 mo) were obtained from breeding institutions and slaughterhouses. The conduction system was dissected from each heart (Fig. 1) and fixed in modified Bouin's (Zamboni's) solution for 16–24 h at 4 °C, as previously described (Crick et al. 1994). Neonatal hearts were also collected from piglets (n = 8; age range, newborn to 4 wk) via a midline sternotomy following an intraperitoneal injection of sodium pentobarbital. This was done in accordance with the *Home Office Guidance on the Operation of the Animals* (*Scientific Procedures*) *Act 1986*. These hearts were not dissected but underwent fixation and cryopreparation in their entirety. Fixed tissue specimens were subsequently rinsed in several changes of 15% (wt/vol) sucrose-phosphate buffered saline solution (PBS; 0.1 M, pH 7.2). Each tissue specimen was placed on a cork mat, covered with mounting medium (Tissue-Tek, Miles Inc., Elkhart, USA), and frozen in isopentane suspended in liquid nitrogen. Neonatal pig hearts were

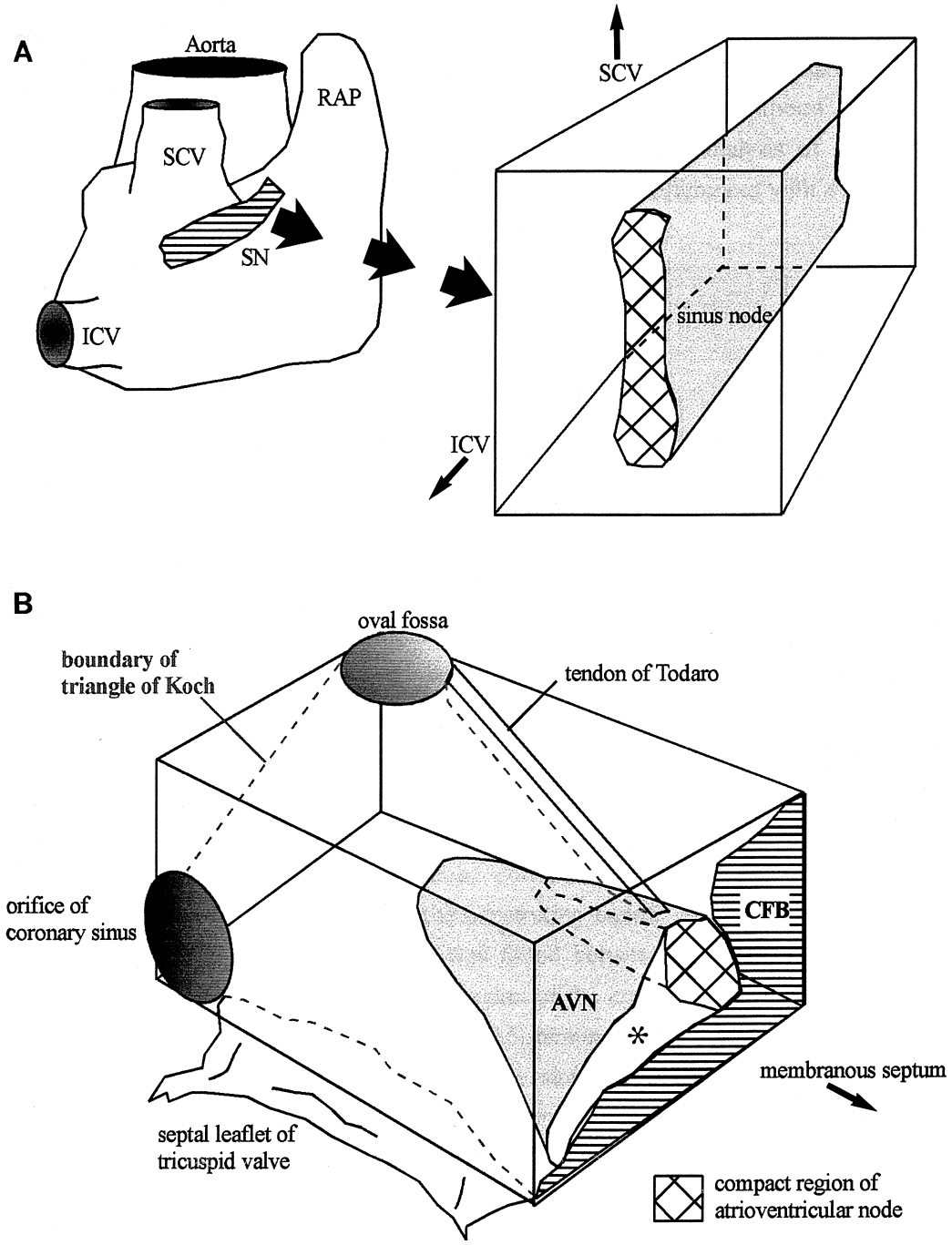


Fig. 1. Schematic diagrams illustrating the morphology, localisation and dissection of the porcine sinus node (*A*) and atrioventricular node (*B*). The porcine sinus node (*A*) is situated within the terminal groove that runs between the junction of the superior caval vein (SCV) and the right atrial appendage (RAP), and is essentially rectangular in its longitudinal appearance. Its tail-end stretches towards the inferior caval vein (ICV). The porcine atrioventricular node is isolated within the landmark of the triangle of Koch, as shown (*B*). The node is triangular in sagittal section, with its transitional region dominating the nodal musculature. SN, sinus node; AVN, atrioventricular node; asterisk, transitional atrioventricular nodal region; CFB, central fibrous body.

oriented either with the atrioventricular junctions lying perpendicular to the cork mat, with the left ventricle facing uppermost (n = 4), or alternatively mounted on their trimmed apexes, with their basal surfaces facing uppermost. Serial cryostat sections (15 μm) were taken through the neonatal hearts and through the cryostat blocks containing adult conduction tissue. In the adult conduction tissues, this resulted in the collection of approximately 800 sections from the sinus nodal region; 800 sections from the atrioventricular nodal region; 150 sections from the penetrating atrioventricular bundle, and a further 150 sections from the proximal regions of the bundle branches.

Table. *Source and characterisation of antisera*

| Antigen | Species | Code | Dilution | Source |
|---|---|---|---|---|
| PGP 9.5 | Human | RA95 | 1:2000 | Ultraclone, UK |
| TH | Bovine | TZ1010 | 1:400 | Eugene Tech Int., USA |
| NPY | Synthetic peptide | 951027B | 1:200 | Biogenesis Ltd. |
| CGRP | Rat | C-8198 | 1:1000 | Sigma, UK |
| VIP | Mammalian | 64-720 | 1:2000 | ICN, UK |
| SOM | Mammalian | SZ1114 | 1:1000 | Eugene Tech Int., USA |

All primary antisera used were polyclonals raised from rabbit.

*Immunostaining*

An indirect immunofluorescence technique was adopted for the visualisation of innervation with the use of primary antisera to the general neural marker protein gene product 9.5 (PGP 9.5), tyrosine hydroxylase (TH), neuropeptide Y (NPY), calcitonin gene-related peptide (CGRP), somatostatin and vasoactive intestinal polypeptide (VIP). These antisera are well-characterised (Table). Cryostat sections were collected on Vectabond-treated slides (Vector Laboratories, Peterborough, UK) and air dried for at least 1 h at room temperature. Sections were immersed in buffered saline containing 0.2% Triton X-100 for 30 min, washed in buffer and then stained with pontamine sky blue (BDH, Poole, UK) for 30 min to reduce background fluorescence and to counterstain elastic tissue. Sections were then washed in buffer to remove excess counterstain and incubated for 16–24 h at 4 °C in diluted primary antisera (see Table). After incubation, the sections were washed in buffer and incubated with fluorescein isothiocyanate-labelled (FITC) goat antirabbit IgG (DAKO, UK) diluted 1:200. Following additional washes, the preparations were mounted in Vectashield-mounting medium (Vector Laboratories) and examined with a Leitz Laborlux S microscope equipped for epillumination. In negative control experiments, no immunofluorescence staining was obtained when sections were incubated without the primary antibody, with preimmune serum as replacement for the primary antibody, or by the preabsorption of optimally diluted antisera with the corresponding antigens ($10^{-5}$–$10^{-6}$ M for 16–24 h at 4 °C).

*Acetylcholinesterase (AChE) staining*

Specific antibodies to either AChE or choline acetyltransferase (ChAT) do not give satisfactory staining of peripheral neural tissue in the heart compared with, for example, that of the enteric nervous system (Schemann et al. 1993). For this reason, a modified AChE histochemical technique (Crick et al. 1994) remains the most feasible technique available to visualise putative cholinergic autonomic nerves in cardiac tissue. Briefly, following the immersion in the incubation solution, AChE activity was visualised by placing sections for 5 min in Tris hydrochloride buffer (50 mM, pH 7.6) containing 0.04% 3, 3′-diaminobenzidine tetrahydrochloride and 0.03% nickel ammonium sulphate, and then for another 5–10 min with the addition of 0.003% hydrogen peroxide. In control experiments, AChE activity was found to be absent following incubation of sections without acetylthiocholine iodide, and following the addition of $10^{-4}$ M eserine (physostigmine, Sigma, St Louis, MO, USA) to the incubating solution.

*Quantification of innervation density*

The relative density of the overall pattern of innervation, and of its specific neural subpopulations, was determined by computer-assisted image analysis of immunofluorescent and AChE-stained preparations using the Quantimet 500+ image processing system (Leica, Cambridge, UK). Immunofluorescent and AChE-stained images were captured via a low-light colour video camera (JVC, model TK-1280E) mounted on a Leitz Laborlux S research microscope. The procedure for the quantification of innervation was similar to that described previously (Crick et al. 1994). Background autofluorescence was kept to a minimum by using optimally diluted antisera, and by counterstaining the sections with pontamine sky blue. A cut-off filter at 560 nm was placed between the microscope and the video camera to eliminate red light, which enhanced the contrast of immunofluorescent images. Similarly, the discrimination of AChE-stained nerves was enhanced by the presence of a green filter between the microscope and the video camera. Intramyocardial blood vessels, nodal arteries, and their associated perivascular nerves were edited from the captured images prior to discrimination, thus preventing variation in the distribution of these

structures from affecting the resultant measurements of percentage stained nerve area. Consequently, comparative measurements were restricted to specific regions of the conduction system and its adjacent myocardium, which were outlined manually. Images were digitised into a $512 \times 512$ pixel array, with each pixel representing one of 256 grey levels. Captured immunofluorescent images were then segmented, by setting the upper threshold to 255, and adjusting the lower threshold to a level whereby the stained nerve fibres represented the brightest regions of the image. AChE-stained captured images were discriminated in a similar manner, although their lower threshold level was set at zero, whilst the upper threshold was raised so that the nerves fibres represented the darkest regions of the image. The process of interactive discrimination (segmentation) was standardised for each neural subpopulation undergoing analysis by adjusting the variable threshold level to a similar value for each measurement (within range $\pm 5$ grey levels). Nerve fibres, small nerve bundles (fascicles) and nerve trunks were quantified, but ganglion cells and paraganglion cells, if present, were excluded from these measurements. All fields of view containing conduction tissue and its adjacent myocardium were analysed, which dispelled the need for random selection. Vectashield-mounting medium can preserve fluorescence during prolonged storage at 4 °C for at least 3 mo. Nevertheless, all sections were quantified within 2 wk of application of the FITC-conjugated secondary antibody. Image analysis was carried out on selected regions of the adult porcine conduction system based on a similar procedure as previously described in the human (Crick et al. 1994) and in the calf heart (Crick et al. 1996*a*). All sections containing conduction tissue from neonatal hearts were analysed.

### *Statistics*

Serial sections corresponding to the same regions in each of the 8 adult and 8 neonatal cases were selected for image analysis. The data are expressed as the mean and 95% confidence interval (95% CI) of the percentage stained nerve area, and are derived from the measurements taken from the conduction systems of the 8 adult pigs. The data from the conduction system of neonatal pigs was compared with that of adults in order to investigate the variation of innervation density from birth to young adulthood. Levels of statistical significance were obtained from analysis of variance (ANOVA) comparisons, following logit transformation of the data. Differences with $P$ values $< 5\%$ were considered significant.

## RESULTS

### *General pattern of innervation*

An abundant supply of PGP 9.5-immunoreactive nerve trunks, nerve fascicles and varicose nerve fibres, representing the total innervation, were distributed throughout the porcine conduction system. Each component of the conduction system possessed a significantly higher density of PGP 9.5-immunoreactive innervation than that of the surrounding atrial or ventricular myocardium ($P < 0.0001$; Fig. 2). No significant differences were observed between the density of the total PGP 9.5-immunoreactive innervation throughout the component structures of the conduction system, with the nodal tissues displaying similar percentage stained nerve areas to the ventricular conduction tissues (Fig. 2). Nevertheless, a differential pattern was demonstrated within the regions of the atrioventricular node, and between the components of the ventricular conduction system, the latter showing a definite gradient in density of nerves from the penetrating bundle to the bundle branches (Fig. 2). No significant difference was found between the percentage stained nerve areas of the sinus node, transitional region of the atrioventricular node, and the penetrating bundle (Fig. 2). Many PGP 9.5-immunoreactive ganglion cell bodies were observed in the peripheral regions of the sinus node and the tissues of the atrioventricular groove. Many nerve trunks originated from the latter cells and proceeded into the atrioventricular node. Most of these ganglion cells were close to the epicardium and were part of an extensive neuronal plexus (see Crick et al. 1999). Ganglion cell bodies were observed within the interstices of the compact atrioventricular node, but were absent from the ventricular conduction system. Large nerve trunks (diameter 150–300 μm) could be traced throughout the entire length of the peripheral regions of the sinus node, and also through the transitional region of the atrioventricular node. The transitional zone of the atrioventricular node was itself innervated by numerous fascicles and varicose nerve fibres, with this pattern of innervation continuing throughout the network of the penetrating atrioventricular bundle, the bundle branches, and their terminal arborisations. The majority of the innervation of these terminal Purkinje fibres was composed of small fascicles and fine varicose fibres.

### *Sinus node*

*Morphology*. The sinus node was situated in the terminal groove at the junction of the superior caval

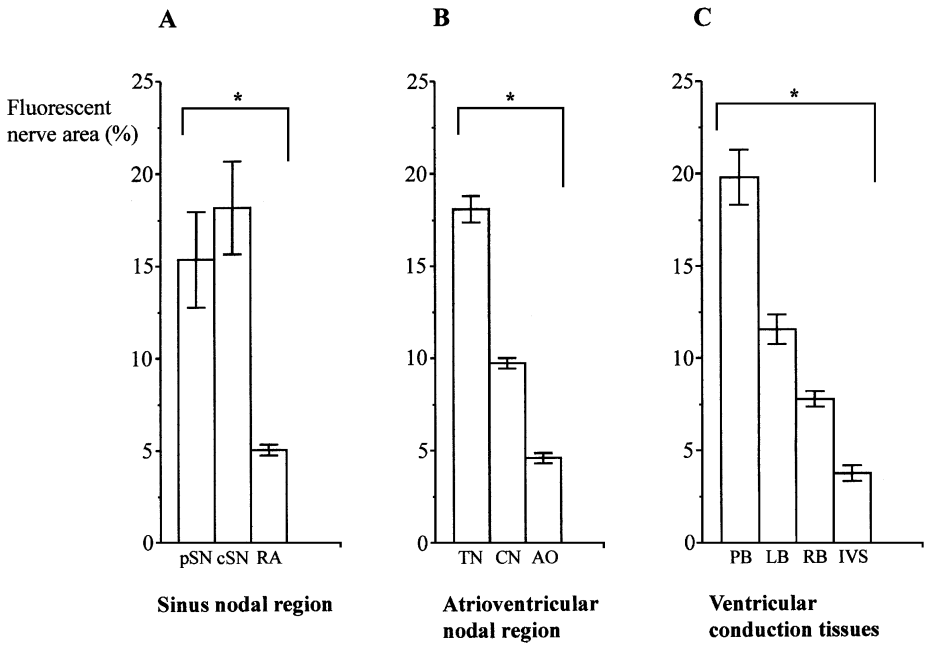


Fig. 2. Bar graphs showing the percentage stained nerve area of PGP 9.5-immunoreactive nerves in sections throughout specific regions of the porcine conduction system in order to compare the distribution of innervation between the sinus node (*A*); atrioventricular node (*B*); ventricular conduction tissues (*C*) and their surrounding myocardial tissues. Each bar represents the mean and 95% confidence interval (95% CI) derived from 8 animals. pSN, peripheral region of the sinus node; cSN, central region of the sinus node; RA, right atrium; TN, transitional region of the atrioventricular node; CN, compact region of the atrioventricular node; AO, atrial overlay tissue adjacent to the node; PB, penetrating atrioventricular bundle; LB, left bundle branch; RB, right bundle branch; IVS, interventricular septum. * $P < 0.0001$.

vein and the right atrial appendage. It had the appearance of a flattened cigar (Fig. 1), and lacked a broad central region such as found in the human sinus node (see Crick et al. 1994). The mean dimensions of nodes in adult hearts (n = 8) were length $18 \pm 2$ mm; maximum width (central nodal region) $3 \pm 0.35$ mm; and minimum width (peripheral nodal region) $2 \pm 0.46$ mm. On average, less than half the thickness of the atrial wall was composed of nodal tissue. The nodal artery was less prominent in the porcine sinus node than that of the human or bovine hearts. The nodal artery entered the nodal tissue at its anterosuperior border, where it divided into at least 2 arterial branches which ramified throughout the entire length of the node to its inferoposterior border. The node itself was composed of small rounded nodal myocytes (diameter 4–7 μm) embedded in an extremely dense fibrous tissue matrix. The fibrous tissue represented approximately 60% of the total nodal area, and surrounded numerous blood vessels. The peripheral regions of the node were histologically similar to the central zone of the node. The border between the nodal tissue and the atrial musculature (diameter atrial myocytes 16–20 μm) was well defined, and similar to that of the human sinus node. Nevertheless, at the inferoposterior border of the node, strands of peripheral nodal myocytes extended for no more than 1 mm into the atrial musculature. No insulated pathways were observed from the node through the right atrial musculature, nor did well innervated tracts emanate from the node.

*Innervation.* The sinus node possessed more than a 3-fold higher density of PGP 9.5-immunoreactive innervation relative to that of the surrounding atrial myocardium ($P < 0.0001$; Fig. 2). No significant difference was found in the total percentage stained area of PGP 9.5-immunoreactive nerves between the central and peripheral nodal regions ($P = 0.1104$; Fig. 2). Large nerve trunks (diameter 200–300 μm) continued throughout the entire length of the node and were more prominent at the nodal borders (Fig. 3). These nerve trunks were often observed to leave the nodal tissue to anastomose with either epicardial ganglia or nerve trunks. Further nerve trunks were then found to re-enter the nodal musculature at other sites (Fig. 3). The majority of PGP 9.5-immunoreactive innervation in the central regions of the node was composed of a complex network of fascicles and varicose fibres. A proportion of the larger nerve trunks were associated with branches of the nodal artery and could, therefore, be described as perivascular nerves.

AChE-positive nerve trunks and fibres (11.74[10.89–12.59]%) represented approximately 65% of the total PGP 9.5-immunoreactive innervation, being by far the most dominant subpopulation

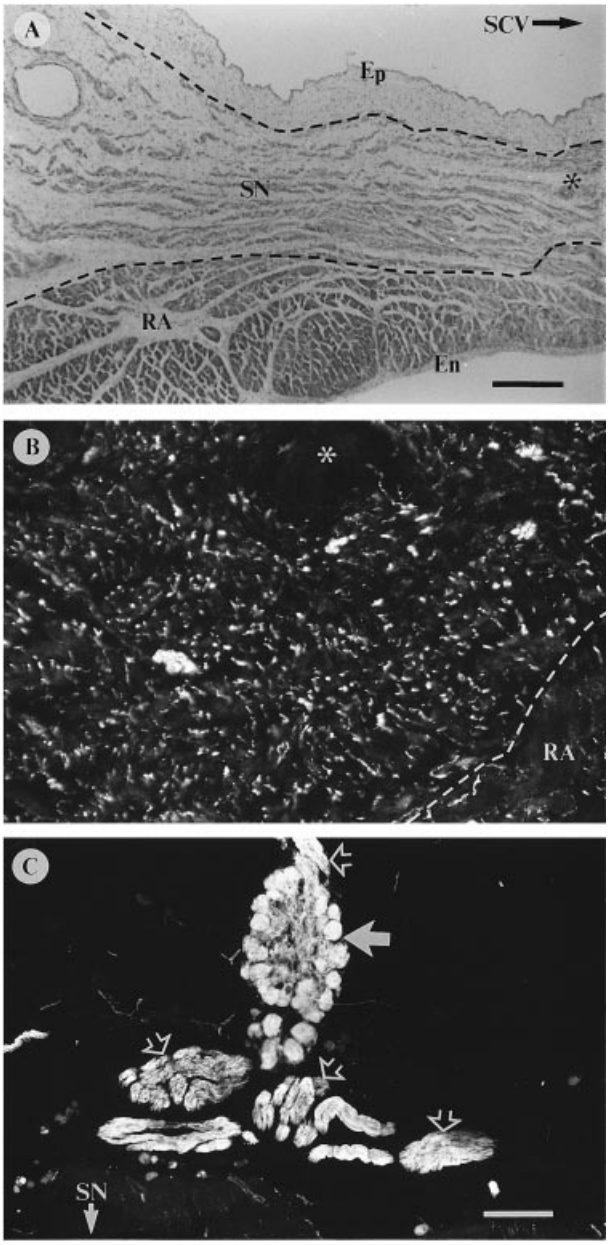


Fig. 3. Photomicrographs of sagittal sections of the sinus node showing the histology (*A*) and distribution of immunoreactivity for PGP 9.5 within the nodal musculature (*B*) and in one of the numerous subepicardial ganglia (closed arrow), with their associated nerve trunks (open arrows) above the node (*C*). SCV, superior caval vein; Ep, epicardial surface; SN, sinus node; RA, musculature of right atrium; En, endocardial surface; * branch of nodal artery. Bars (*A*) 500 μm; (*B*, *C*) 100 μm.

within the node ($P < 0.0001$; Figs 4 *a*, 5). A large proportion of nerve trunks running throughout the nodal tissue, and all ganglion cell bodies, demonstrated AChE activity. Most of the ganglionated nerve trunks surrounding the epicardial surface of the node also displayed AChE-positive profiles.

Large TH-immunoreactive nerve trunks were also observed running adjacent to AChE-positive nerve trunks located within the nodal tissue but close to the border with the atrial musculature, and also at the nodal surfaces adjacent to both the superior caval vein and the terminal crest. No ganglion cell bodies displayed TH immunoreactivity. TH immunoreactivity was detected in a significantly lower proportion of nerve trunks and fibres (5.65[4.87–6.42]%) than that for AChE activity ($P < 0.0001$), representing approximately 30% of the total nodal innervation (Fig. 4*b*). Axonal profiles of TH immunoreactivity were found in nerve trunks that also possessed AChE-positive nerves in adjacent sections (Fig. 5).

NPY-immunoreactive nerves were distributed in similar fashion, and occupied an insignificant difference of percentage stained nerve area to that of TH-immunoreactive nerves ($P = 0.4230$; Fig. 4*b*). This NPY-immunoreactive subpopulation represented the predominant peptidergic nerve supply within the node. No ganglion cell bodies demonstrated immunoreactivity for NPY. Immunoreactivity for CGRP was localised to isolated nerve fibres within AChE-positive nerve trunks, to varicose nerve fibres around non-immunoreactive ganglion cell bodies, and to isolated varicose fibres scattered between nodal myocytes. CGRP-immunoreactive nerve fibres (Fig. 4*c*) occupied a significantly lower percentage stained area (1.55[1.23–1.88]%; $P < 0.0001$) than the subpopulation of nerves immunoreactive for NPY, and represented approximately 8% of the total neural population. Somatostatin-immunoreactive nerves were relatively sparse in comparison to either NPY or CGRP-immunoreactive nerves, representing less than 4% of the overall innervation (Fig. 4*d*). They were mostly found in the peripheral regions of the node and surrounding unreactive epicardial ganglion cells. Nerve fibres displaying immunoreactivity for VIP were rare, their distribution being too sparse to permit accurate analysis. When found, these fibres were closely associated with small blood vessels, mainly arterioles, within the nodal tissue and also, to a lesser extent, in the atrial myocardium.

### *Atrioventricular node*

*Morphology*. The atrioventricular node was located in a similar position to that of the human and bovine hearts, that is at the apex of the triangle of Koch (Fig. 1). The triangle of Koch was situated in a more inferior position within the septal musculature of the right atrium compared with that of the human heart, and this contrasting feature reflecting the different atrial morphology between the 2 species (see Crick et al. 1998). The nodal length in adult pigs was approximately $15 \pm 2.5$ mm ($n = 8$) when measured

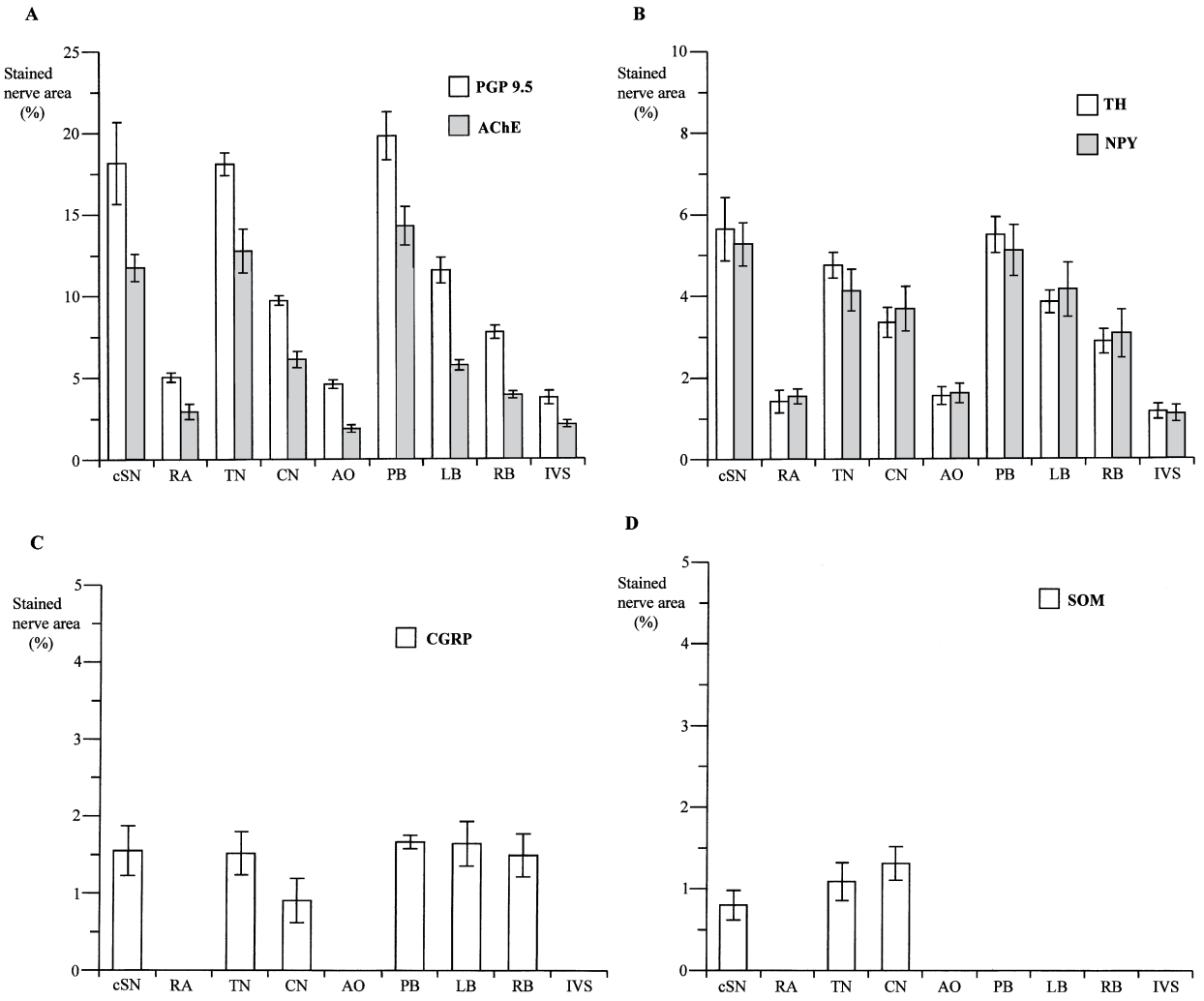


Fig. 4. Bar graphs of percentage stained nerve area of PGP 9.5-immunoreactive and AChE-positive nerves (*A*); TH and NPY-immunoreactive nerves (*B*); CGRP-immunoreactive nerves (*C*); and somatostatin (SOM)- and VIP-immunoreactive nerves (*D*) throughout specific regions of the porcine conduction system. Each bar represents the mean and 95% confidence interval (95% CI) derived from 8 animals. cSN, central region of the sinus node; RA, right atrium; TN, transitional region of the atrioventricular node; CN, compact region of the atrioventricular node; AO, atrial overlay tissue adjacent to the node; PB, penetrating atrioventricular bundle; LB, left bundle branch; RB, right bundle branch; IVS, interventricular septum.

from the first myocytes of the transitional zone to the penetration of the axis into the central fibrous body. In morphological terms, the node was not arranged as a half-oval abutting the central fibrous body, as in the human atrioventricular node; in contrast, the porcine node appeared as a sheet-like structure, with an almost triangular appearance in sagittal section (Figs 1, 6). The nodal structure possessed 2 histologically distinct zones: the compact nodal region, situated adjacent to the central fibrous body, and the more extensive transitional nodal region, which coursed from its atrial myocardial border and passed over the compact nodal region on its right border, finally impinging onto the hingepoint of the septal leaflet of the tricuspid valve (Fig. 6). There was no observable anatomical barrier separating these 2 nodal regions. In contrast, the transitional zone of the human atrioventricular node surrounds an extensive compact node in a circumferential manner, creating the characteristic half-oval structure (Crick et al. 1994). The transitional zone also extended towards the more distal regions of the node, impinging on the axis at the point at which it pierced the membranous septum to become the penetrating atrioventricular bundle. The transitional zone was composed of spindle-shaped cells that often merged with each other to form a 'Purkinje fibre-like' network embedded in a dense fibrous tissue matrix. These spindle-shaped cells were smaller than the atrial myocytes (diameter 15–20 μm), but significantly larger than the more rounded cells of the compact node (diameter 5–10 μm). The compact nodal region itself was significantly smaller than the transitional zone and was located close to, but not astride, the central fibrous body. The left superior

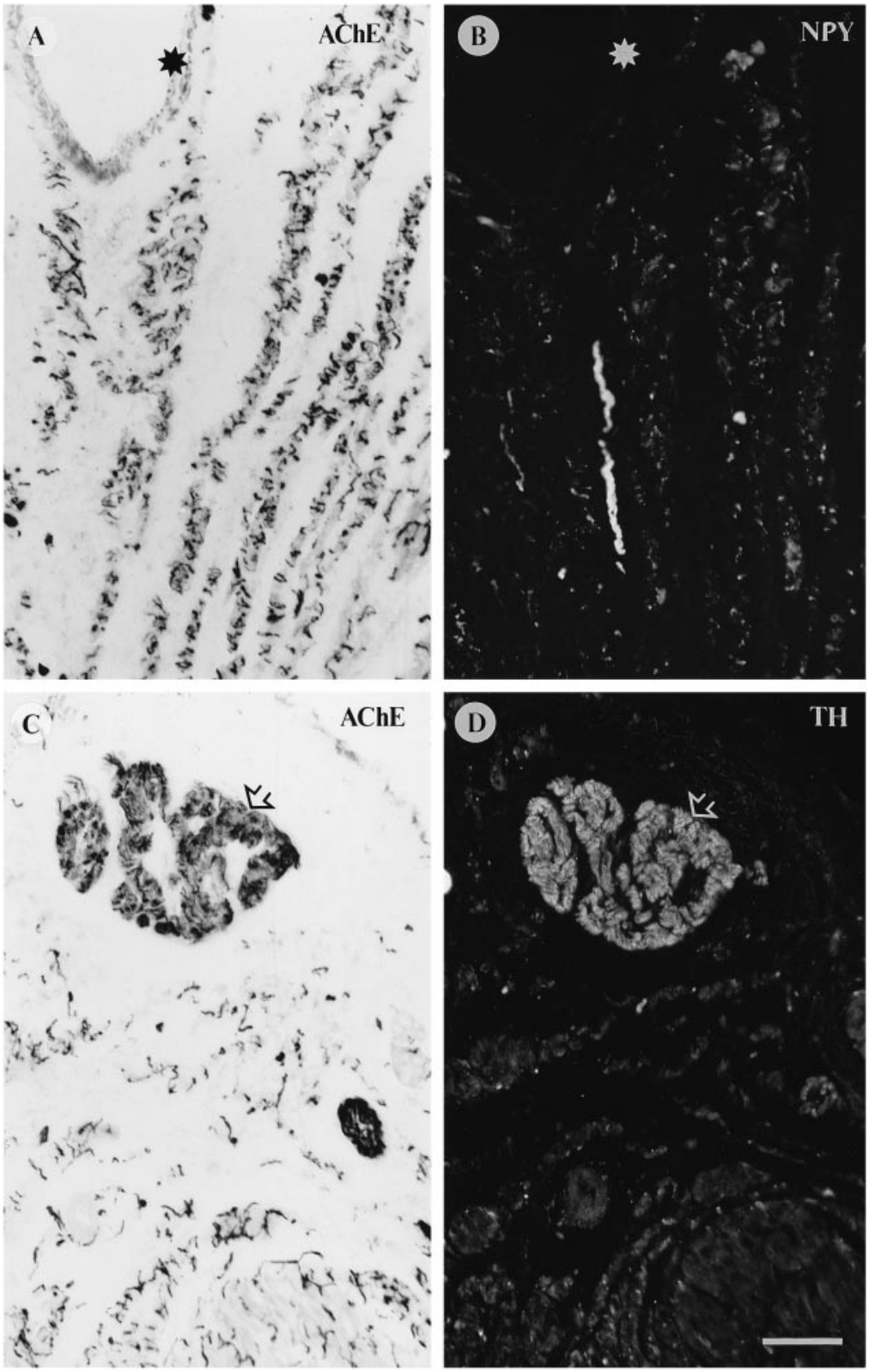


Fig. 5. Photomicrographs demonstrating the distribution patterns of AChE-positive innervation (*A*, *C*) and nerves displaying immunoreactivity for NPY (*B*) and TH (*D*) in the sinus node. NPY-immunoreactive and AChE-positive nerves are shown to display contrasting patterns of distribution in adjacent sections (*A*, *B*: star indicates same nodal artery). A nerve trunk (open arrows) is seen to possess both AChE-positive and TH-immunoreactive nerve profiles which have differing localisation patterns in adjacent sections. Bar, 100 μm.

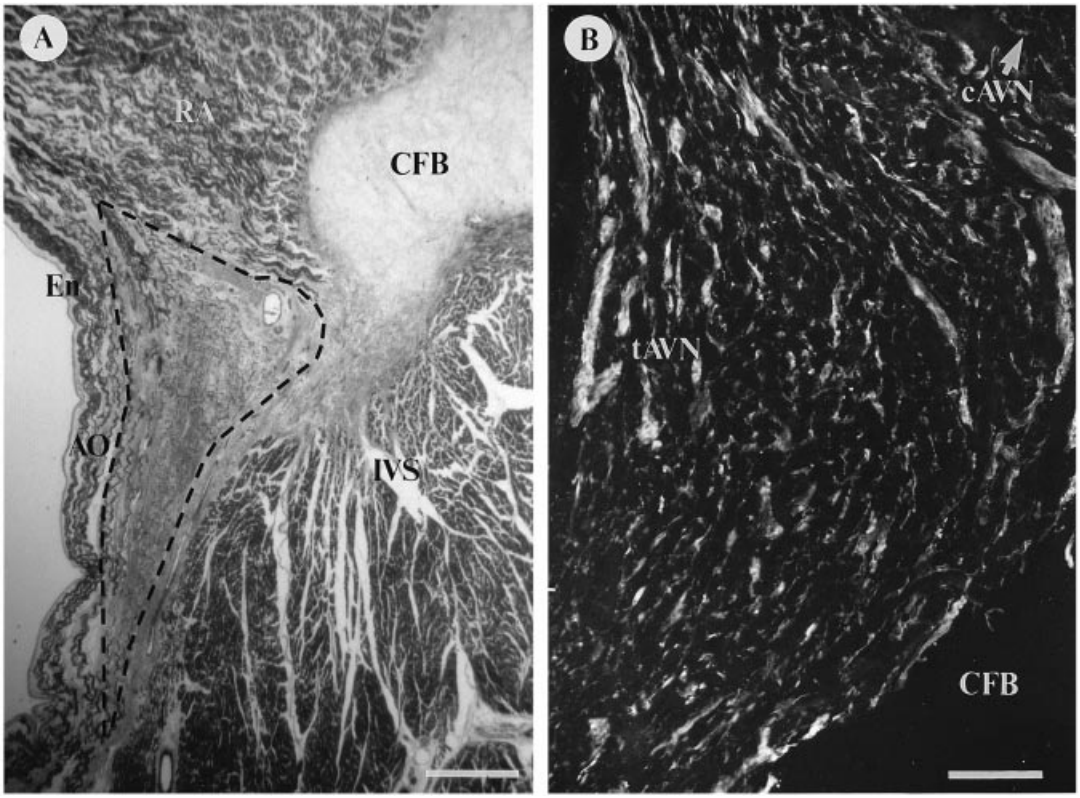


Fig. 6. Photomicrographs illustrating the histology (Masson's trichrome stain; *A*) and pattern of PGP 9.5-immunoreactive innervation of the atrioventricular node (*B*). The node is triangular in sagittal section, with the majority of the nodal musculature being composed of transitional atrioventricular myocytes (tAVN). A proportion of the compact nodal region abuts the central fibrous body (CFB). RA, musculature of the floor of the right atrium; En, endocardial surface; AO, atrial overlay tissue of node; IVS, interventricular septum; cAVN, compact region of atrioventricular node. Bars, (*A*) 1000 μm; (*B*) 100 μm.

surface of the compact node was, therefore, observed to be in direct contact with the musculature of the right atrium (Fig. 6). Tapering strands of transitional nodal cells were observed at the most posterior extremities of the node, extending towards the coronary sinus and becoming interwoven with bundles of atrial myocytes. Nonetheless, as in the human and bovine hearts, these did not represent insulated tracts running through the atrial musculature. This was proven in serial sections of neonatal pig hearts, where examination of the entire atrial tissues revealed no morphological evidence of internodal insulated pathways.

*Innervation*. A rich supply of PGP 9.5-immunoreactive trunks and fascicles entered the atrioventricular node at its posterior border from the atrioventricular groove, the floor of the right atrium, and a small proportion from the perivascular innervation associated with branches of the atrioventricular nodal artery. Numerous PGP 9.5-immunoreactive ganglia were observed in the epicardial tissues of the atrioventricular groove, and also in both the transitional nodal zone, and compact nodal region, where they were found in conjunction with nerve trunks that coursed the entire length of the node (Fig. 6). The transitional nodal region possessed a numerous supply of nerve trunks, fascicles and varicose fibres whereas, in comparison, the compact nodal region possessed mainly small nerve fascicles and a dense network of varicose fibres (Fig. 6). Both nodal regions possessed a significantly higher relative density of PGP 9.5-immunoreactive innervation than the atrial musculature adjacent to the node ($P < 0.0001$; Fig. 2). No significant difference was observed between the percentage stained area of PGP 9.5-immunoreactive innervation of the transitional atrioventricular nodal region and that of the sinus node ($P = 0.9487$). The transitional nodal region (18.09[17.40–18.77]%), however, possessed a 2-fold higher percentage stained area of PGP 9.5-immunoreactive nerves than did the compact nodal region (9.72[9.44–9.99]%) ($P < 0.0001$; Fig. 2). The rich innervation of the transitional nodal region continued throughout the entire axis of the node, extending to the point where it pierced the fibrous tissue of the membranous septum to become the penetrating atrioventricular bundle. A characteristic feature observed in all atrioventricular nodes was the presence of 3–4 large nerve trunks located at the border between the 2 nodal zones which coursed along the

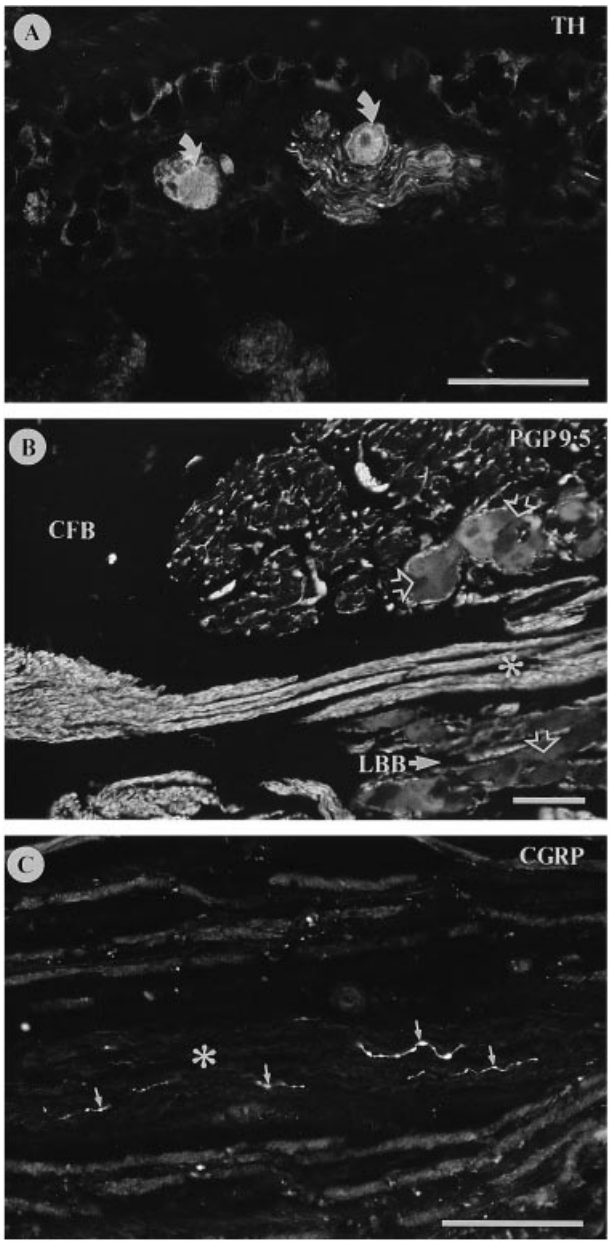


Fig. 7. Immunofluorescent photomicrographs showing ganglion cell bodies (curved closed arrows) in the atrioventricular nodal region displaying immunoreactivity for TH (*A*), together with the distribution of PGP 9.5 (*B*) and CGRP (*C*) immunoreactive nerve supplying the Purkinje fibres (open arrows) of the left bundle branch (LBB). The same nerve trunk (*) contains varicose fibres immunoreactive for CGRP (small arrows, *C*). CFB, central fibrous body. Bar, 100 μm.

entire nodal axis from its posterior border towards the membranous septum. These nerve trunks were traced posteriorly to ganglia within the atrioventricular groove.

AChE-positive nerves were the dominant subpopulation observed in both nodal regions, representing a 2-fold higher density relative to TH and NPY-immunoreactive nerves ($P < 0.0001$; Fig. 4 *a*, *b*). As in the sinus node, the majority of nerve trunks and fascicles in the transitional nodal region displayed AChE activity, together with all ganglion cell bodies located within the atrioventricular groove and in the tissues surrounding the node. The transitional nodal region (12.76[11.41–14.12]%) possessed a 2-fold higher density of AChE-positive nerves compared with the subpopulation observed in the compact nodal region (6.08[5.58–6.58]%). These nerves represented approximately 70% and 60% of the total innervation within the transitional and compact nodal regions, respectively.

After AChE-positive innervation, the next most abundant neural subpopulation displayed immunoreactivity for TH. TH immunoreactivity in the transitional nodal region (4.76[4.45–5.07]%) was localised mostly to trunks, fascicles and a minor subpopulation of ganglion cell bodies (Fig. 7), and represented approximately 25% of the total innervation (Fig. 4*b*). TH-immunoreactive nerves represented a larger proportion, approximately 35%, of the total innervation in the compact nodal region (3.35[2.99–3.71]%), where immunoreactivity was localised to small fascicles and varicose fibres. The distribution pattern of TH-immunoreactive nerves was different to the localisation of AChE-positive nerves in adjacent sections.

The dominant peptidergic nerve supply displayed immunoreactivity for NPY, which demonstrated a similar percentage stained area and distribution pattern to that of TH-immunoreactive nerves in adjacent sections of both nodal regions (Fig. 4*b*). No immunoreactivity for NPY was observed in ganglion cell bodies, although immunoreactive varicose fibres were observed surrounding cell bodies, and NPY-immunoreactive axonal profiles were observed within nerve trunks associated with neuronal ganglia. CGRP immunoreactivity in both parts of the node was localised to varicose nerve fibres, and to isolated axonal profiles within nerve trunks that were themselves found to be predominantly AChE-positive in adjacent sections. CGRP-immunoreactive nerve fibres represented approximately 8–9% of the total neural population in both nodal regions. The transitional nodal region possessed a significantly higher relative density of CGRP-immunoreactive fibres compared to the compact nodal region ($P = 0.0026$; Fig. 4*c*). Somatostatin immunoreactivity was localised to isolated varicose nerve fibres which demonstrated a different pattern of distribution to that of either NPY or CGRP- immunoreactive nerves. No significant difference ($P = 0.1805$) was observed in the percentage stained area of somatostatin-immunoreactive nerve fibres between the transitional (1.09[0.86–1.32]%) and compact (1.31[1.10–1.51]%) nodal regions (Fig. 4*d*).

Nevertheless, a larger somatostatin-immunoreactive subpopulation was apparent in the compact nodal region, representing approximately 13% of the total innervation, whereas these nerves represented less than 6% of the total innervation pattern of the transitional nodal region. Somatostatin-immunoreactive nerve fibres were closely associated with AChE-positive nerve fibres, but were not found to be co-localised either in adjacent sections or on examination of sequentially stained sections. Somatostatin immunoreactivity was also displayed by varicose fibres surrounding immunoreactive ganglion cell bodies within the atrioventricular groove. VIP-immunoreactive nerves were again relatively sparse in comparison with other peptidergic nerves, representing less than 1% of the total innervation of the atrioventricular node.

*Ventricular conduction tissues*

*Morphology*. After piercing the central fibrous body, the interwoven spindle-shaped cells of the conduction axis became larger and more rounded to form the penetrating atrioventricular bundle. Initially, the proximal atrioventricular bundle was composed of cells similar to those of the extensive transitional regions of the atrioventricular node. Indeed, from examination of serial sections, it became apparent that the greater part of the penetrating atrioventricular bundle could be traced in a posterior direction to the terminal regions of the transitional atrioventricular node. Only a small proportion of the compact nodal region appeared to be in contact with the proximal regions of the penetrating atrioventricular bundle. The majority of this structure, therefore, was formed by the transformation of the spindle-shaped transitional cells of the node into the larger Purkinje fibres, which often anastomosed with each other. The Purkinje fibres of the proximal atrioventricular bundle were larger (diameter 60–70 μm) than the transitional nodal cells, and these increased in size (diameter 90 μm) as the penetrating bundle progressed into the branching bundle and ultimately into its subdivisions of the left and right bundle branches. The exact point of divergence of the branching bundle into its 2 branches was somewhat offset in the pig compared with man, reflecting the extent of muscular support of the aortic valve. This, in turn, influences the relative position of the membranous septum within the outflow tract (see Crick et al. 1998).

*Innervation*. All component tissues of the ventricular conduction system possessed a significantly higher density of PGP 9.5-immunoreactive nerves than the musculature of the surrounding interventricular septum ($P < 0.0001$; Fig. 2). The penetrating atrioventricular bundle possessed numerous PGP 9.5-immunoreactive nerve trunks and fascicles that coursed between the Purkinje fibres and surrounded the many anastomoses that interconnected these fibres. This pattern continued throughout the proximal regions of the bundle branches, but in more distal regions the pattern of innervation was characterised by smaller fascicles and varicose fibres. Ganglion cell bodies were not observed in these tissues. The penetrating atrioventricular bundle (19.81[18.34–12.27]%) possessed an approximately 2-fold and 3-fold higher density of PGP 9.5-immunoreactive nerves than the left (11.55[10.74–12.37]%) and right (7.78[7.37–8.18]%) bundle branches, respectively ($P < 0.0001$; Fig. 2). The penetrating atrioventricular bundle possessed the highest mean percentage area value of PGP 9.5–immunoreactive nerves of the entire conduction system, although this was not significantly different when compared with the mean values for either the sinus node or the transitional atrioventricular nodal region ($P = 0.1634$; Fig. 2).

AChE-positive nerve trunks and fibres were the dominant neural subtype observed in the penetrating atrioventricular bundle (14.28[13.09–15.46]%), and in both the left (5.72[5.40–6.04]%) and right (3.89[3.65–4.13]%) bundle branches, where they represented 72%, 49.5% and 50% of the total innervation, respectively (Fig. 4*a*). The majority of the nerve trunks coursing through the atrioventricular bundle were AChE-positive, and this contributed to the significantly higher percentage stained nerve area observed here compared with either of the 2 bundle branches ($P < 0.0001$; Fig. 4*a*). Very few AChE-positive varicose nerve fibres were observed in the penetrating atrioventricular bundle, but were much more apparent surrounding the Purkinje fibres of the bundle branches. AChE-positive nerves were also the dominant neural population within the surrounding ventricular septal musculature, but these nerves represented a significantly lower density than any region of the ventricular conduction system ($P < 0.0001$).

In all regions of the ventricular conduction system, TH-immunoreactive nerves represented a significantly lower proportion of the total innervation than those found to be AChE-positive ($P < 0.0001$). They represented 28%, 33% and 37% of the total innervation pattern in the penetrating atrioventricular bundle (5.49[5.04–5.94]%), left bundle branch (3.85[3.58–4.13]%), and right bundle branch (2.88[2.58–3.19]%)

respectively, and again displayed a different pattern of distribution to AChE-positive nerves. Despite this, the penetrating atrioventricular bundle possessed a significantly higher percentage stained area of TH-immunoreactive nerves than either of the 2 bundle branches ($P < 0.0001$; Fig. 5*b*). TH immunoreactivity was localised to smaller nerve fascicles and to varicose fibres. Again, some TH-immunoreactive nerve profiles were observed within predominantly AChE-positive nerve trunks.

NPY-immunoreactive nerves displayed a similar percentage stained area (Fig. 4*b*) and pattern of distribution to that of TH immunoreactivity in adjacent sections ($P = 0.3017$). They represented the dominant peptidergic subpopulation within these tissues. After NPY, varicose nerve fibres immunoreactive for CGRP represented the next most abundant neural subtype. Similar percentage nerve areas of CGRP-immunoreactive nerve fibres were present in the penetrating atrioventricular bundle (1.67[1.59–1.76]%), and in both left (1.65[1.36–1.94]%), and right (1.50[1.21–1.78]%) bundle branches ($P = 0.4936$) (Fig. 4*c*). Nevertheless, the bundle branches possessed a much higher proportion of these nerves (14–19%), compared with that of the penetrating atrioventricular bundle (8%). Some CGRP-immunoreactive nerve fibres were observed in nerve trunks with predominantly AChE-positive axonal profiles. Nerve fibres immunoreactive for either somatostatin or VIP were not observed in any region of the ventricular conduction system or its surrounding musculature.

### *Neonatal hearts*

The innervation of the conduction system in neonatal porcine hearts (n = 5; mean age, $20 \pm 2.5$ d) was found to be quantitatively comparable with the data obtained from the young adult hearts. Both the sinus and atrioventricular nodes possessed similar percentage stained areas of PGP 9.5 and NPY- immunoreactive, and AChE-positive nerves, to that found in the adult hearts (Fig. 8).

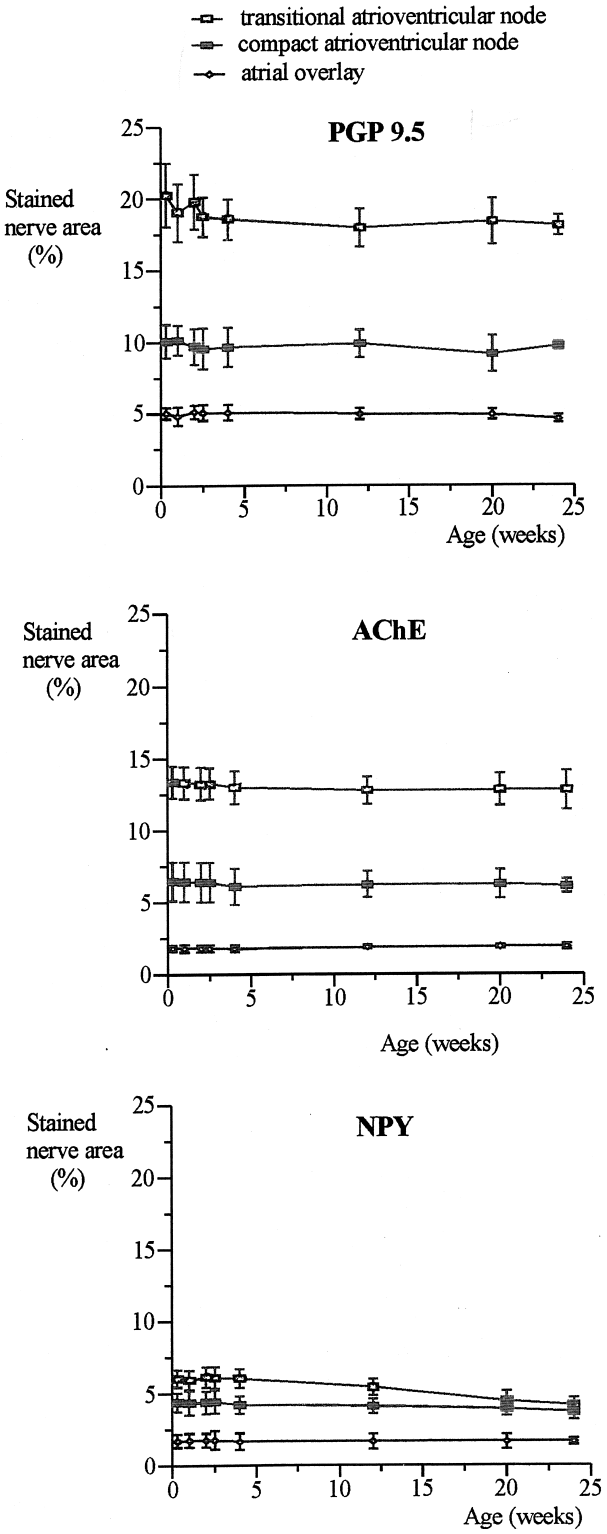


Fig. 8. Plots showing the effect of age on the percentage stained area of nerves displaying immunoreactivity for PGP 9.5, activity for AChE and immunoreactivity for NPY in the porcine atrioventricular node. Each bar represents the mean and 95% confidence interval derived from the hearts of neonatal animals of the following age ranges: newborn (n = 1); 1 d (n = 1); 1 wk (n = 2); 3 wk (n = 1); 4 wk (n = 3) and the 8 adult animals (age range 3–6 mo).

## DISCUSSION

We have found a differential autonomic innervation of the porcine conduction system, as visualised by the general neural marker PGP 9.5, the rank order in relative neural density being transitional atrioventricular node, sinus node and atrioventricular penetrating bundle > left bundle branch > compact atrioventricular node and right bundle branch ≫

myocardial tissues. This gradient is similar to that described in the bovine conduction system (Crick et al. 1996*a*). Similarities also exist in the mean density of PGP 9.5-immunoreactive nerves between the nodal tissues of the human and porcine heart, but the markedly higher density of innervation of the penetrating atrioventricular bundle and the ventricular conduction tissues of the pig creates difficulties in matching their respective patterns of innervation (Crick et al. 1994).

The porcine sinus node possessed an almost homogeneous distribution of PGP 9.5-immunoreactive nerve trunks, fascicles and fibres throughout its length. Variations in the morphology of the porcine sinus node were found compared with that of man. Most important was the thin, elongated shape of the porcine node compared with the human node. Electrophysiological investigations have revealed that the porcine sinus node is characterised by unifocal impulse generation (Crick et al. 1996*a*), whereas multifocal impulse generation is characteristic for the human and canine nodes (Boineau et al. 1990). This functional difference correlates well with the uniform distribution of innervation observed in the porcine sinus node compared with the variation observed in the human node (Crick et al. 1994). Large ganglionated nerve trunks were observed to course throughout the entire length of the peripheral nodal regions, especially on their epicardial borders, and were similar to those observed in the sinus node of the bovine heart (Crick et al. 1996*a*). This may indicate that a substantial proportion of nerves innervating the node are either of intrinsic origin or, alternatively, are in synaptic contact with intracardiac ganglia (Priola, 1980).

The dense innervation of both the atrioventricular node and the ventricular conduction system was, as indicated, similar to that of the bovine heart, but markedly different from that of the human heart. The morphology of the porcine electrocardiogram is also known to be different from that of man. Thus, the QRS duration (39 ms) and QT interval (260–310 ms) of the adult pig heart (Hughes, 1986) are much shorter than the durations observed in the human heart, which are 80–120 ms and 350–450 ms, respectively (Timmis, 1988). The contrasting morphology and histology of the porcine atrioventricular nodal and ventricular conduction tissues compared with that of man may account for these electrophysiological differences. Additionally, the efficiency of electrical coupling between the cells of the transitional atrioventricular nodal region and Purkinje system may also explain this phenomenon. A recent study in the rat atrioventricular node demonstrated a differential expression of $\beta$-adrenoreceptor subtypes between the transitional and midnodal cell regions suggesting that subtype-specific neuromodulators may have distinct effects on atrioventricular conduction (Petrecca & Shrier, 1998). The study by Petrecca & Shrier (1998) illustrated their findings by demonstrating differential patterns of parasympathetic and sympathetic innervation within the atrioventricular node, from which they concluded that a multiplicity of sites for modulation of impulse conduction may exist within this region. Nevertheless, this merits further investigation. The rich supply of nerves in the transitional region of the atrioventricular node was similar to that observed in the bovine heart (Crick et al. 1996*a*), and would ensure that functional delay of impulse conduction through the atrioventricular node was under stringent autonomic regulation. The observation of populations of ganglion cell bodies within the musculature of the compact atrioventricular nodal region has important implications for the neural regulation of the porcine node. Ganglion cell bodies are absent from the atrioventricular node of both the human (Crick et al. 1994) and bovine heart (Crick et al. 1996*a*), but are present in the guinea pig (Crick et al. 1996*b*). The presence of intrinsic cardiac ganglia within the atrioventricular nodal axis indicates that intrinsic neurons comprise an important component of the overall pattern of innervation. An extensive ganglionated plexus has been characterised electrophysiologically in the neonatal pig heart (Smith et al. 1992). It may follow, therefore, that the ganglion cell bodies within the atrioventricular node may be involved in local integrative circuits and local reflexes that could be receptive to changes in the rate of impulse propagation or changes in the electrical activity of its nodal cells (Moravec et al. 1986; Allen & Burnstock, 1987; Moravec & Moravec 1987; Gagliardi et al. 1988; Ardell et al. 1991; Selyanko & Skok, 1992). A high density of innervation was also observed in the Purkinje fibre network of the atrioventricular penetrating bundle and bundle branches, similar to the pattern of distribution observed in the bovine heart (Crick et al. 1996*a*). It is tempting to speculate that this high density of innervation may be required to modulate the fast electrical coupling observed throughout the Purkinje system.

The rank order of immunoreactive nerve subtypes, expressed as a proportion of PGP 9.5-immunoreactive innervation, throughout the porcine conduction system was AChE (60–70 %) > TH and NPY (25–35 %) > CGRP (8–19 %) > somatostatin (less than 13 %)

> VIP (less than 1 %). AChE-positive nerves were by far the most dominant subpopulation throughout the porcine conduction system. The majority of ganglion cell bodies also possessed activity for AChE. This may indicate that a substantial proportion of AChE-positive innervation within the porcine conduction system can be considered intrinsic in origin, comparable to the innervation of the bovine conduction system (Crick et al. 1996*a*). It is tempting to speculate that the higher density of AChE-positive nerves within these tissues, as a proportion of the total innervation pattern, may indicate the presence of a more extensive intrinsic innervation pattern than in the human conduction system (Crick et al. 1994). Nevertheless, this can only be accurately assessed by measuring the density of residual innervation following total efferent decentralisation of the heart, which has not been carried out in the pig.

The density of TH-immunoreactive nerves was significantly lower than that of AChE-positive innervation throughout all regions of the conduction system. TH-immunoreactive nerve profiles were sometimes observed in the same nerve trunks as AChE-positive nerves, supporting the view of Forsgren (1988) that presumptive sympathetic fibres do travel in conjunction with presumptive parasympathetic fibres. These large nerve trunks did not appear to be associated with intracardiac ganglia, and probably represent efferent postganglionic nerves. The presence of TH-immunoreactive ganglion cell bodies within the atrioventricular nodal region indicates the ability of porcine intrinsic neurons to synthesise catecholamines, and this correlates well with the reported effect of noradrenaline on synaptic transmission within a subpopulation of intrinsic neurons of the pig (Smith et al. 1992), rat (Moravec & Moravec, 1989), and dog (Butler et al. 1990). TH-immunoreactive cell bodies have also been described in the bovine heart (Gordon et al. 1993*a*), and the fetal human heart (Gordon et al. 1993*b*), but have not been reported to be present in the adult human heart either before or after transplantation (Wharton et al. 1990). NPY-immunoreactive nerves represented the predominant peptidergic subpopulation throughout the porcine conduction system and they display a similar pattern of distribution to TH-containing nerves, as in other mammalian hearts (Forsgren, 1989; Wharton et al. 1990; Gordon et al. 1993*a*, *b*; Crick et al. 1996*a*, *b*). Despite this pattern of colocalisation, NPY immunoreactivity was not demonstrated in any of the ganglion cell bodies that were immunoreactive for TH. Nevertheless, a minor subpopulation of cultured intracardiac neurons from fetal human hearts has been reported to display immunoreactivity for NPY (Hassall et al. 1990). This may, of course, be a consequence of the culture conditions, but the paucity of NPY-immunoreactive cell bodies in porcine intracardiac ganglia suggests that species differences may be responsible for these contrasting patterns of distribution.

Nerves immunoreactive for CGRP were observed in both the nodal and ventricular conduction tissues, where they possessed an almost uniform pattern of distribution. This pattern was similar to that observed in the guinea pig conduction system (Crick et al. 1996*b*). Their density was significantly lower than that of NPY-immunoreactive nerves but the proportion of CGRP-immunoreactive nerves in the ventricular conduction system was relatively high compared with other nerve subtypes. CGRP is thought to be localised to sensory afferent fibres in the mammalian heart (Franco-Cereceda et al. 1987; Forsgren, 1994), but their relative density varies between species, which is thought to be responsible for the differences observed in its action in the heart (Wharton et al. 1988). CGRP has been reported to be involved in the attenuation of vagal responses in the heart since it is known to affect the activity of intracardiac vagal ganglia (Xi et al. 1989). This correlates well with the finding of CGRP-immunoreactive varicose fibres in predominantly AChE-positive nerve trunks that were observed in the ventricular conduction tissues.

In comparison with other peptidergic nerve subpopulations, somatostatin-immunoreactive nerves were relatively sparse. They were only found in the sinus node and the transitional region of the atrioventricular node. A minor subpopulation of ganglion cell bodies was observed to possess immunoreactivity for somatostatin indicating that this peptide in the pig, as in the human heart (Day et al. 1985), may be localised to intrinsic neurons. Their density was relatively higher than those observed in the human conduction system (Crick et al. 1994), but they were found in similar regions, such as the transitional atrioventricular node. Since the porcine atrioventricular node was observed to possess a significant intracardiac nerve supply, and with the knowledge that somatostatin depresses atrioventricular nodal conduction, then it may follow that this peptide is important in the intrinsic neural regulation of the porcine node (Webb et al. 1986). Even though the actions of somatostatin closely resemble that of vagal stimulation (Franco-Cereceda et al. 1986), no colocalisation was observed with AChE-positive nerves. This suggests that, unlike the human heart, somatostatin-immunoreactive nerves may not represent post-

ganglionic parasympathetic neurons (Franco-Cereceda et al. 1986), providing further evidence of the variation in the pattern of innervation in the porcine conduction system to that of the human heart. This variation also extends to the relative sparsity of VIP-immunoreactive nerves compared with their density in the human conduction system (Crick et al. 1994).

In terms of the effect of maturation on the density of innervation in the conduction system, no significant variation was observed in either the density of PGP 9.5-immunoreactive or AChE-positive nerves within the atrioventricular node. A slight decrease in the density of NPY-immunoreactive nerves was observed between newborn piglets and young adults of 25 wk. Nevertheless, this was restricted to the transitional region of the atrioventricular node and was not observed elsewhere. This lack of variation with age is consistent with the lack of variation observed in the fetal, neonatal and adult human heart (Gordon et al. 1993*b*; Chow et al. 1993, 1995). It has been suggested that cardiac innervation is intact at the 24 wk stage of gestation of the human fetus (Gordon et al. 1993*b*), and remains constant through to at least the neonate (Chow et al. 1993).

In summary, we have described several important differences in the pattern of distribution of autonomic innervation between the conduction system of the pig and that of other mammalian species, including man. A substantial proportion of nerve fibres innervating the nodal tissues could be traced from intracardiac ganglia, indicating the presence of an extensive intrinsic supply. Both the innervation, and overall morphology, of the atrioventricular node were markedly different to that of the human heart. The pig heart is known to be very susceptible to ventricular arrhythmias (Hughes, 1986). This, together with the knowledge that the porcine conduction system, in particular the atrioventricular node, possesses an extensive intracardiac neural supply, capable of functioning independently of efferent innervation (Smith et al. 1992; Murphy et al. 1994; Armour et al. 1998), may have implications for the physiology of a donor pig heart within the human recipient. It is important that we are aware of these findings in view of the future use of transgenic pig hearts for human xenotransplantation.

## ACKNOWLEDGEMENTS

The authors express their thanks to Dr Alison Hislop, Dr Joan Deutsch and Professor S. G. Haworth (Institute of Child Health, London, UK) for providing us with a number of neonatal pig hearts. Dr Crick was funded by a grant from the British Heart Foundation. Dr Ho and Professor Anderson are supported by the British Heart Foundation together with the Joseph Levy Foundation.

## REFERENCES

ALLEN TG, BURNSTOCK G (1987) Intracellular studies of the electrophysiological properties of cultured intracardiac neurons of the guinea pig. *Journal of Physiology* **388**, 349–366.

ARDELL JL, BUTLER CK, SMITH FM, HOPKINS DA, ARMOUR JA (1991) Activity of in vivo atrial and ventricular neurons in chronically decentralized canine heart. *American Journal of Physiology* **260**, H713–H721.

ARMOUR JA, MURPHY DA, YUAN BX, MACDONALD S, HOPKINS DA (1997) Gross and microscopic anatomy of the human cardiac nervous system. *Anatomical Record* **247**, 289–298.

ARMOUR JA, COLLIER K, KEMBER G, ARDELL JL (1998) Differential selectivity of cardiac neurons in separate intrathoracic autonomic ganglia. *American Journal of Physiology* **274**, R939–949.

BOINEAU JP, SCHEUSSLER RB, CAIN ME, CORR PB, COX JL (1990) Activation mapping during normal atrial rhythms and atrial flutter. In *Cardiac Electrophysiology*: *From Cell to Bedside* (ed. Zipes DP, Jalife JJ), pp. 537–547. Philadelphia: W. B. Saunders.

BOWMAN TA, HUGHES HC (1984*a*) Swine as an in vivo model for electrophysiologic evaluation of cardiac pacing parameters. *PACE* **7**, 187–194.

BOWMAN TA, HUGHES HC (1984*b*) Ventriculoatrial conduction in swine during cardiac pacing: animal model for retrograde conduction. *American Heart Journal* **108**, 337–341.

BUTLER CK, SMITH FM, CARDINAL R, MURPHY DA, HOPKINS DA, ARMOUR JA (1990) Cardiac responses to electrical stimulation of discrete loci in canine atrial and ventricular ganglionated plexi. *American Journal of Physiology* **259**, H1365–H1373.

CHOW LT, CHOW SS, ANDERSON RH, GOSLING JA (1993) Innervation of the human cardiac conduction system at birth. *British Heart Journal* **69**, 430–435.

CHOW LT, CHOW SS, ANDERSON RH, GOSLING JA (1995) The innervation of the human myocardium at birth. *Journal of Anatomy* **187**, 107–114.

COOPER DKC, YE Y, ROLF LL, ZUHDI N (1991) The pig as potential organ donor for man. In *Xenotransplantation*: *The Transplantation of Organs and Tissues Between Species* (eds. Cooper DKC, Kemp E, Reemtsma K, White DJG), pp. 480–500. Berlin: Springer.

COZZI E, WHITE DJG (1995) The generation of transgenic pigs as potential organ donors for humans. *Nature Medicine* **1**, 964–966.

CRICK SJ, WHARTON J, SHEPPARD MN, ROYSTON D, YACOUB MH, ANDERSON RH et al. (1994) Innervation of the human cardiac conduction system. A quantitative immunohistochemical and histochemical study. *Circulation* **89**, 1697–1708.

CRICK SJ, SHEPPARD MN, ANDERSON RH, POLAK JM, WHARTON J (1996*a*) A quantitative assessment of innervation in the conduction system of the calf heart. *Anatomical Record* **245**, 685–698.

CRICK SJ, SHEPPARD MN, ANDERSON RH, POLAK JM, WHARTON J (1996*b*) A quantitative study of nerve distribution in the conduction system of the guinea pig heart. *Journal of Anatomy* **188**, 403–416.

CRICK SJ, SHEPPARD MN, HO SY, GEPSTEIN L, ANDERSON RH (1998) Anatomy of the pig heart: comparisons

with normal human cardiac structure. *Journal of Anatomy* **193**, 105–119.

CRICK SJ, ANDERSON RH, HO SY, SHEPPARD MN (1999) Localization and quantitation of autonomic innervation in the porcine heart II: endocardium, myocardium and epicardium. *Journal of Anatomy* **195**, 359–373.

DAY SM, GU J, POLAK JM, BLOOM SR (1985) Somatostatin in the human heart and comparison with guinea pig and rat heart. *British Heart Journal* **53**, 153–157.

DE BIASI S, VITELLARO-ZUCCARELLO L (1982) Intrinsic innervation of porcine semilunar heart valves. *Anatomy and Embryology* **65**, 71–79.

DE BIASI S, VITELLARO-ZUCCARELLO L, BLUM I (1984) Histochemical and ultrastructural study on the innervation of human and porcine atrioventricular valves. *Anatomy and Embryology* **169**, 159–165.

DOUGLAS WR (1972) Of pigs and men and research: a review of applications and analogies of the pig, *Sus scrofa*, in human medical research. *Space Life Sciences* **3**, 226–234.

FORSGREN S (1988) The distribution of terminal sympathetic nerve fibres in bundle branches and false tendons of the bovine heart. An immunohistochemical and catecholamine histofluorescence study. *Anatomy and Embryology* **177**, 437–443.

FORSGREN S (1989) Neuropeptide Y-like immunoreactivity in relation to the distribution of sympathetic nerve fibres in the heart conduction system. *Journal of Molecular & Cellular Cardiology* **21**, 279–290.

FORSGREN S (1994) Distribution of calcitonin gene-related immunoreactivity in the bovine conduction system. Correlation with substance P. *Regulatory Peptides* **52**, 7–19.

FRANCO-CERECEDA A, LUNDBERG JM, HÖKFELT T (1986) Somatostatin: an inhibitory parasympathetic transmitter in the human heart? *European Journal of Pharmacology* **132**, 101–102.

FRANCO-CERECEDA A, HENKE H, LUNDBERG JM, PETERMANN JB, HÖKFELT T, FISCHER JA (1987) Calcitonin gene-related peptide (CGRP) in capsaicin-sensitive substance P-immunoreactive sensory neurons in animals and man. Distribution and release by capsaicin. *Peptides* **8**, 399–410.

GAGLIARDI M, RANDALL WC, BEIGER D, WURSTER RD, HOPKINS DA, ARMOUR JA (1988) Activity of in vivo canine cardiac plexus neurons. *American Journal of Physiology* **255**, H789–H800.

GORDON L, WHARTON J, GAER JAR, INGLIS GC, TAYLOR KM, POLAK JM (1993*a*) Quantitative immunohistochemical assessment of bovine myocardial innervation before and after cryosurgical cardiac denervation. *Cardiovascular Research* **27**, 318–326.

GORDON L, POLAK JM, MOSCOSO GJ, SMITH A, KUHN DM, WHARTON J (1993*b*) Development of the peptidergic innervation of human heart. *Journal of Anatomy* **183**, 131–140.

HASSALL CJS, PENKETH R, RODECK C, BURNSTOCK G (1990) The intracardiac neurons of the fetal human heart in culture. *Anatomy and Embryology* **182**, 329–337.

HOPKINS DA, GOOTMAN PM, GOOTMAN N, DI RUSSO SM, ZEBALLOS ME (1984) Brainstem cells of origin of the cervical vagus and cardiopulmonary nerves in the neonatal pig (Sus scrofa). *Brain Research* **306**, 63–72.

HUGHES HC (1986) Swine in cardiovascular research. *Laboratory Animal Science* **36**, 348–350.

MACDONALD AA, POOT P, WENSING JG (1983) Nerve endings in the pulmonary trunk, ductus arteriosus and aorta of intact and decapitated pig fetuses. *Anatomy and Embryology* **168**, 395–404.

MORAVEC M, COURTALON A, MORAVEC J (1986) Intrinsic neurosecretory neurons of the rat heart atrioventricular junction: possibility of local neuromuscular feed back loops. *Journal of Molecular and Cellular Cardiology* **18**, 357–367.

MORAVEC J, MORAVEC M (1987) Intrinsic nerve plexus of the mammalian heart: morphological basis of cardiac rhythmical activity. *International Review of Cytology* **106**, 89–148.

MORAVEC M, MORAVEC J (1989) Adrenergic neurons and short proprioceptive feedback loops involved in the integration of cardiac function in the rat. *Cell & Tissue Research* **258**, 381–385.

MURPHY DA, O'BLENES S, HANNA BD, ARMOUR JA (1994) Capacity of intrinsic neurons to modify the acutely autotransplanted mammalian heart. *Journal of Heart & Lung Transplantion* **13**, 847–856.

OPTHOF T, DE JONGE B, JONGSMA HJ, BOUMAN LN (1987) Functional morphology of the pig sinoatrial node. *Journal of Molecular & Cellular Cardiology* **19**, 1221–1236.

PETRECCA K, SHRIER A (1998) Spatial distribution of nerve processes and beta-adrenoreceptors in the rat atrioventricular node. *Journal of Anatomy* **192**, 517–528.

PRIOLA DV (1980) Intrinsic innervation of the canine heart. Effects on conduction in the atrium, atrioventricular node, and proximal bundle branch. *Circulation Research* **47**, 74–79.

SCHEMANN M, SANN H, SCHAAF C, MÖDER M (1993) Identification of cholinergic neurons in enteric nervous system by antibodies against choline acetyltransferase. *American Journal of Physiology* **265**, G1005–G1009.

SELYANKO AA, SKOK VI (1992) Synaptic transmission in rat cardiac neurons. *Journal of the Autonomic Nervous System* **39**, 191–200.

SINGH S, JOHNSON PI, LEE RE, ORFEI E, LONCHYNA VA, SULLIVAN HJ et al. (1996) Topography of cardiac ganglia in the adult human heart. *Journal of Thoracic & Cardiovascular Surgery* **112**, 943–953.

SMITH FM, HOPKINS DA, ARMOUR JA (1992) Electrophysiological properties of in vitro intrinsic cardiac neurons in the pig (*Sus scrofa*). *Brain Research Bulletin* **28**, 715–725.

TIMMIS AD (1988) The electrocardiogram and chart X-ray. *Essentials of Cardiology*, pp. 29–30. Oxford: Blackwell Scientific.

TRANUM-JENSEN J (1975) The ultrastructure of the sensory end-organs (baroreceptors) in the atrial endocardium of young mini-pigs. *Journal of Anatomy* **119**, 255–275.

WEBB SC, KRIKLER DM, HENDRY WG, ADRIAN TE, BLOOM SR (1986) Electrophysiological actions of somatostatin on the atrioventricular junction in sinus rhythm and reentry tachycardia. *British Heart Journal* **56**, 236–241.

WHARTON J, GULBENKIAN S, MERIGHI S, KUHN DM, JAHN R, TAYLOR KH et al. (1988) Immunohistochemical and ultrastructural localisation of peptide-containing nerves and myocardial cells in the human atrial appendage. *Cell & Tissue Research* **254**, 155–166.

WHARTON J, POLAK JM, GORDON L, BANNER NR, SPRINGALL DR, ROSE M et al. (1990) Immunohistochemical demonstration of human cardiac innervation before and after transplantation. *Circulation Research* **66**, 900–912.

WHITE D, WALLWORK J (1993) Xenografting: probability, possibility or pipe-dream? *Lancet* **342**, 879–880.

XI X, DUFF MJ, WEBER M, FISCUS BI, THOMAS JX, O'TOOLE MF et al. (1989) In vivo effects of calcitonin gene-related peptide (CGRP) on intracardiac vagal ganglia (Abstract). *FASEB Journal* **3**, A413.